Measurement of 3D Motion of Myocardial Material Points from Explicit B-Surface Reconstruction of Tagged MRI Data

Amir A. Amini, Petia Radeva, Mohamed Elayyadi, and Debiao Li

CVIA Lab, Box 8086, 660 S. Euclid,
Washington University Medical Center,
St. Louis, MO 63110-1093,
email: amini@mobius.wustl.edu
home page: http://www-cv.wustl.edu

Abstract. MRI is unique in its ability to non-invasively and selectively alter tissue magnetization, and create tag planes intersecting image slices. The resulting grid of signal voids allows for tracking deformations of tissues in otherwise homogeneous-signal myocardial regions. In this paper, we propose a specific Spatial Modulation of Magnetization (SPAMM) imaging protocol together with efficient techniques for measurement of 3D motion of material points of the human heart from images collected with the SPAMM method. The techniques make use of tagged images in orthogonal views by explicitly reconstructing 3D B-spline surface representation of each tag plane (two intersecting the short-axis (SA) image slices and one intersecting the long-axis (LA) image slices). The developed methods allow for viewing deformations of 3D tag surfaces, spatial correspondence of long-axis and short-axis image slice and tag positions, as well as non-rigid movement of myocardial material points as a function of time.

1 Introduction

Non-invasive techniques for assessing the dynamic behavior of the human heart are invaluable in the diagnosis of heart disease, as abnormalities in the myocardial motion sensitively reflect deficits in blood perfusion [12]. MRI is a non-invasive imaging technique that provides superb anatomic information with excellent spatial resolution and soft tissue contrast. Conventional MR studies of the heart provide accurate measures of global myocardial function, chamber volumes and ejection fractions, and regional wall motions and thickening. In MR tagging, the magnetization property of selective material points in the myocardium are altered in order to create tagged patterns within a deforming body such as the heart muscle. The resulting pattern defines a time-varying curvilinear coordinate system on the tissue. During tissue contractions, the grid patterns move, allowing for visual tracking of the grid intersections over time. The intrinsic high spatial and temporal resolutions of such myocardial analysis schemes provide unsurpassed information about local contraction and deformation in the heart wall

which can be used to derive local strain and deformation indices from different myocardial regions.

Previous work for analysis of tagged images includes work by Young, Kraitchman, Dougherty, and Axel [11] who adopted an analysis system for tagged images based on snakes. Once the tag positions on the myocardium are found, coordinates of these points in deformed images are determined within a volumetric finite element model fitted to endocardial and epicardial contours. The work of Park, Metaxas, and Axel [9] considers geometric primitives which are generalization of volumetric ellipsoids, through use of parameter functions which allow for spatial variations of aspect ratios of the model along the long axis of the LV. This model is specially useful for computing the twisting motion of the heart. Prince and McVeigh and Gupta and Prince developed an optical flow based approach to the analysis of tagged MR images [4]. The approach of Guttman, Prince, and McVeigh [5] for analysis of radial tagged images is to use a graph-search technique that determines the optimal inner and outer boundaries of the myocardium as well as tag lines by finding points one after the other in a sequence, using initial search starting points on the determined LV boundaries. In Amini, Curwen, and Gore [1, 2], tag lines are tracked with Dynamic Programming B-snakes and coupled B-snake grids. Spline warps then warp an area in the plane such that snake grids obtained from two SPAMM frames are brought into registration, interpolating a dense displacement vector field. A volumetric B-solid model was proposed in Radeva, Amini, and Huang [10] to concurrently analyze and track tag lines in different image slices by implicitly defined B-surfaces which align themselves with tagged data. The solid is a 3D tensor product B-spline whose isoparametric curves deform under image forces from tag lines in different image slices. In [6], tag surfaces were constructed using thin-plate splines, and subsequently intersection of the thin-plate spline surfaces were computed based on an alternating projection algorithm to yield displacements of material points.

Although the latter 2 articles provide novel techniques for computation of tag surfaces from discrete image slices, the former paper ([10]) can not reconstruct tag surfaces independent of a B-solid. The latter article ([6]) leads to a somewhat compute intensive algorithm for tag surface reconstruction; in particular requiring inversion of the thin-plate spline matrix [3] of order $O(n \times n)$ (n being the total number of tag points on all image slices.) It is not difficult to see that n can approach upwards of 200. Furthermore, intersecting thin-plate spline surfaces has to be performed in the Euclidean space since the surfaces are not of parametric form. The present article provides machinery for very fast computation of tag surfaces using B-snakes on individual slices, does not require *a priori* computation of a solid, and furthermore since by design the surfaces are parametric, it leads to a naturally easy to implement algorithm for computing 3D material points.

2 Reconstruction of Tag Planes from Coupled B-Snake Grids

B-splines are suitable for representing a variety of industrial and anatomical shapes [1, 7, 8]. The advantages of B-spline representations are: (1) They are smooth, continuous parametric curves which can represent open or closed curves. For our application, due to parametric continuity, B-splines will allow for sub-pixel localization of tags, (2) B-splines are completely specified by few control points, and (3) Individual movement of control points will only affect their shape locally. In medical imaging, local tissue deformations can easily be captured by movement of individual control points without affecting static portions of the curve.

A B-spline curve is expressed as

$$\alpha(u) = \sum_{i=0}^{N-1} p_i B_i(u) \tag{1}$$

where $B_i(u)$ are the B-spline basis functions having polynomial form, and local support, and p_i are the sequence of control point of the B-spline curve. Two remarks should be made regarding the sequence of control points: a) The number of control points is much fewer in number than a sampling of the curve $\alpha(u)$ on a pixel grid, and b) p_i rarely reside on the actual curve. To localize a tag line based on B-snakes, an external energy can be defined and optimized in order to locate feature points on individual image slices [1, 10]. Given a spatial stack of m curves on m image slices, each represented by n control points, a matrix of control points is constructed as follows:

$$\begin{bmatrix} V_{11} & \cdots & V_{1n} \\ & \cdots & \\ V_{m1} & \cdots & V_{mn} \end{bmatrix} \tag{2}$$

where the second index may denote ordering along the x axis, and the first index may denote ordering along the z axis (image slices). The matrix immediately gives rise to the surface

$$S(u,v) = \sum_{ij} V_{ij} B_{i,k}(u) B_{j,k}(v) \tag{3}$$

where we have used non-periodic blending functions as defined in [8]. We have applied cubic splines (i.e., of order $k = 4$) to ensure that there is the necessary flexibility in parametrized shapes (it should be noted that $B_{j,k}$ takes on an identical form to $B_{i,k}$). Furthermore, given that tag lines and images are of approximately equal distance, uniform B-splines are considered so that the knots are spaced at consecutive integer values of parametric variables.

Figures 1 and 2 illustrate the construction of intersecting cubic B-spline tag surfaces from a spatial stack of coupled B-snake grids.
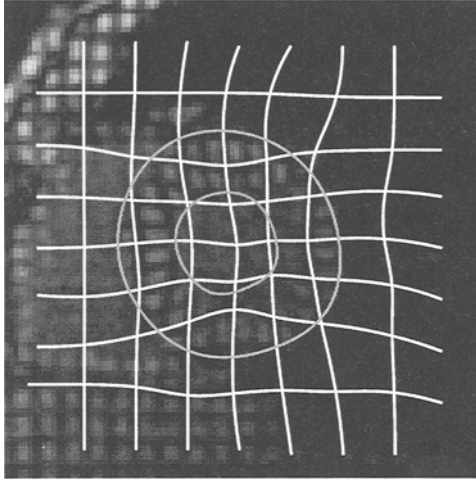
Fig. 1. A grid of B-spline snakes on short-axis image slices in mid-systole. Note that for better illustration, in this figure as well as all analysis to follow every second tag line is utilized. The analysis area of interest is the region within the myocardial borders of the LV.
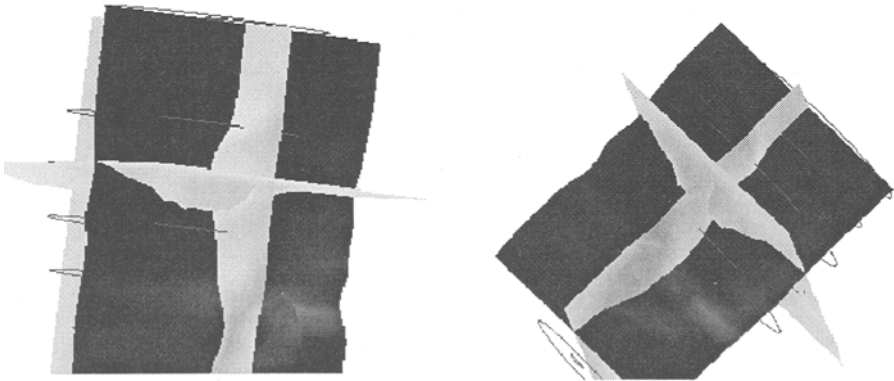

Fig. 2. Figure illustrates the reconstruction of two orthogonal tag surfaces from a sequence of coupled B-spline curves in short-axis image slices (as in figure 1). Two views of the same tag planes are shown. The dark surface corresponds to the second vertical grid line from the right in figure 1. The bright vertical surface orthogonal to this surface corresponds to the fourth horizontal grid line from the top. Finally, the bright horizontal surface is the long-axis tag plane corresponding to the short-axis image slice.

3 Non-Rigid Tracking

The procedure outlined in section 2 provides a mechanism for tracking points within short-axis image slices. However, as shown in figure 3, in MRI, position of image slices are fixed relative to the magnet's coordinate system, and therefore this approach can only yield within short-axis-slice motion of material points. To obtain information about movement of points in the "out-of-plane" direction, a second sequence of images is acquired with slices parallel to the heart's long-axis and with the requirement that tag planes intersecting the new slices be in parallel to short axis images. This requirement however is not sufficient for 3D tracking, and there should yet be an additional requirement, namely that the same set of material points should be imaged in both views. The imaging protocol in section 3.1 accomplishes this goal.
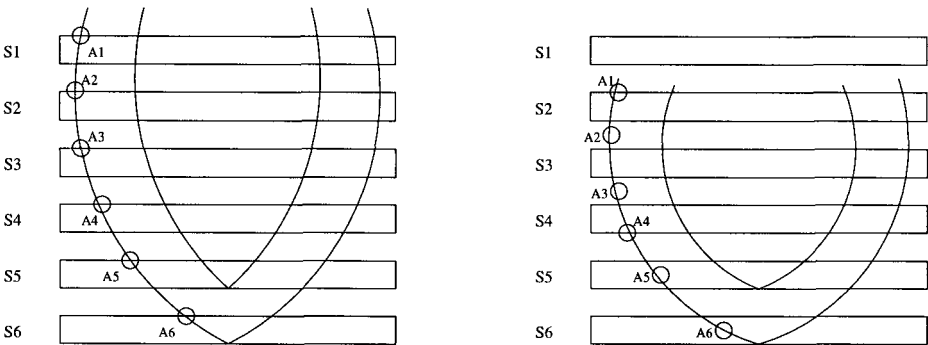

Fig. 3. Imaging geometry in MRI. The position of slices $(S1, \cdots, S6)$ are fixed relative to the magnet's coordinate system. However, a dynamic organ such as the heart moves in-and-out of the slices. Motion of points $A1, \cdots, A6$ illustrates this.

3.1 Imaging Protocol

A SPAMM pulse sequence was used to collect images of normal healthy volunteers. Multiple images in both short-axis and long axis views of the heart were collected to cover the entire volume without gaps. Immediately after the ECG trigger, rf tagging pulses were applied in two orthogonal directions. The repetition time (TR) of the imaging sequence was approximately 7.1 msec, the echo time (TE) was 2.9 msec, the rf pulse flip angle was 15 degrees, and the time extent of rf tag pulses was 22 msec. Echo sharing was used in collecting each time-varying image sequence for given slice position (called a Cine sequence). Five data lines were collected for any time frame during each heart cycle, but two data lines were overlapped between two consecutive cardiac frames, resulting in an effective temporal resolution of approximately 22 *msec*. Other imaging parameters were: field of view $= 330mm$, data acquisition matrix size $= 160 \times 256$

(phase encoding by readout), in-plane resolution $= 2.1 \times 1.3mm^2$, slice thickness $= 7mm$, and tag spacing $= 7mm$. The total imaging time was therefore 32 heart beats for each Cine sequence, and the subject was instructed to breath only following each Cine acquisition. Since there were 19 volumetric temporal frames and 17 spatial slices in each image volume, all of the images were acquired in 544 heartbeats. In the long-axis view, there were also 19 temporal frames. However, 13 slices covered the entire heart in this case resulting in 416 heart beats of total imaging time.

The image orientations for the short-axis and long-axis views of the heart were first determined by collecting multiple oblique angle scout images. For the short-axis images, one of the tagging planes was placed parallel to the long-axis imaging planes of the heart by manually setting the angles of the tagging plane in the coordinate system of the magnet to be the same as those of the long-axis view as determined from scout images. The coordinates of the center of the central tagging plane in the reference coordinates system (relative to the center of the magnet) were set to be the same as those of the center of one of the long-axis image planes to be acquired, again determined by the scout images. As a result, one set of tagging planes intersecting short-axis image slices coincided with long-axis images since both tag spacing and slice thickness were 7 mm center-to-center. The other short-axis tagging plane was placed orthogonal to the first tagging plane. Similarly, long-axis images were acquired with their tag planes coinciding with short-axis slice positions. Figure 4 displays position of the short-axis image slices on one long-axis image at end-diastole.
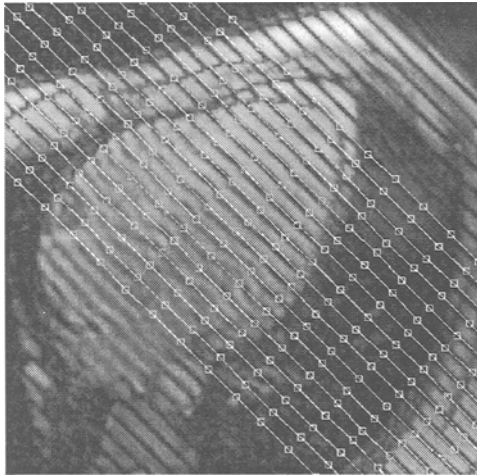

Fig. 4. Position of short-axis image slices at the time of tag placement is drawn on a long-axis image acquired at the same time point in the heart cycle.

As a result of the imaging protocol outlined in this section, the tag intersections from short-axis images are the material points corresponding precisely

to the intersection of three tag planes, and revealing for all time points in the cardiac cycle, 3D motion of these special points.

3.2 Computing Time-Dependent Coordinates of Material Points

As we did in the case of coupled B-snakes of short-axis images, once again we measure deformations of tag planes in the long-axis orientation by creating B-spline surfaces from stacks of B-snakes. The difference between short-axis and long-axis image acquisitions is however that there is only one set of parallel tag planes intersecting long-axis images. Figure 5 illustrates a tag surface constructed from a spatial sequence of long-axis images.
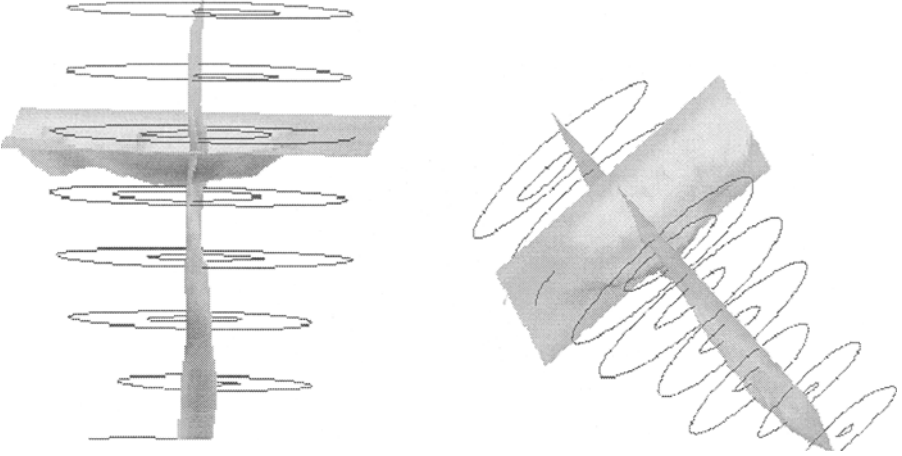
Fig. 5. B-spline surface representation of a long-axis tag plane reconstructed from a spatial stack of B-snakes. Two views of a reconstructed long-axis tag surface is displayed horizontally. "Out-of-plane" movement of the heart is visualized by deviation from flatness of the long-axis B-surface.

Coordinates of material points may be obtained by computing intersections of three intersecting B-spline surfaces representing three intersecting tag surfaces. For each triplet of intersecting B-spline surfaces, $(S_1(u_1, v_1), S_2(u_2, v_2), S_3(u_3, v_3))$, the following computation is carried out

$$\min_{P_1, P_2, P_3} d^2(S_1, S_2) + d^2(S_1, S_3) + d^2(S_2, S_3) \qquad (4)$$

where point P_i belongs to surface S_i and d is the Euclidean distance metric. The minimization is carried out using the method of Conjugate Gradient Descent

which insures fast convergence of the method. Note that the overall distance function above can be written as

$$
\begin{aligned}
&||S_1(u_1, v_1) - S_2(u_2, v_2)||^2 + \\
&||S_2(u_2, v_2) - S_3(u_3, v_3)||^2 + \\
&||S_1(u_1, v_1) - S_3(u_3, v_3)||^2
\end{aligned}
\tag{5}
$$

with the goal of finding the parameters (u_i, v_i) for the triplet of surfaces. The computed parameters will in fact be surface parameters of the intersection point. For the iterative optimization process, a good initial set of parameters has been found to be parameters of the intersection point assuming linear B-spline bases. The algorithm was tested on an image sequence which included 17 slices and 19 frames (17×19 images) yielding temporal position of around 250 material points over the heart cycle. In a movie of these material points, the 3D motion of individual SPAMM points of the myocardium is clearly apparent.

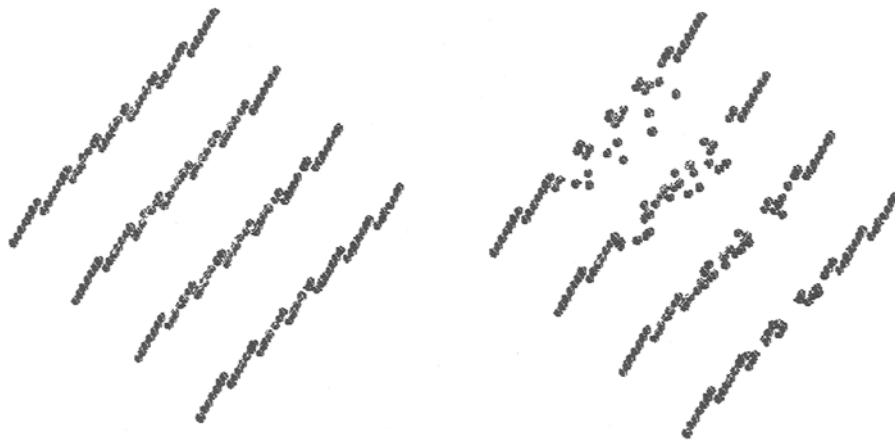Figure 6 displays results of the intersection computation for few of the material points.

Fig. 6. Location of the material points for every fourth slice of the MRI data is displayed on the left. New computed location of material points one-third through systole is shown on the right. Non-rigid motion of material points of the heart can be appreciated: points further up in slices (around the base) move downwards, whereas points near the heart's apex are relatively stationary.

4 Conclusions

In conclusion, we have described efficient methods for visualization and tracking of 3D material points of the heart from 2 sets of orthogonal tagged MR views.

We have argued that in comparison to other forms of tag representation, use of B-splines has several advantages, including immediate generation of tag surfaces, subpixel accuracy for tag plane localization and parametric continuity, as well as the need to only assign the location of few control points in order to determine the location of a complete tag plane. Currently, the system is being used in actual clinical situations as part of a large clinical study.

Acknowledgements

References

1. A. A. Amini, R. W. Curwen, and John C. Gore. Snakes and splines for tracking non-rigid heart motion. In *European Conference on Computer Vision*, pages 251–261, University of Cambridge, UK, April 1996.
2. A. A. Amini and et al. Energy-minimizing deformable grids for tracking tagged MR cardiac images. In *Computers in Cardiology*, pages 651–654, 1992.
3. F. Bookstein. Principal warps: Thin-plate splines and the decomposition of deformations. *IEEE Transactions on Pattern Analysis and Machine Intelligence*, PAMI-11:567–585, 1989.
4. S. Gupta and J. Prince. On variable brightness optical flow for tagged MRI. In *Information Processing in Medical Imaging (IPMI)*, pages 323–334, 1995.
5. M. Guttman, J. Prince, and E. McVeigh. Tag and contour detection in tagged MR images of the left ventricle. *IEEE Transactions on Medical Imaging*, 13(1):74–88, 1994.
6. W. Kerwin and J. Prince. Generating 3-D cardiac material markers using tagged mri. In *Information Processing in Medical Imaging (IPMI)*, pages 313–326, 1997.
7. S. Menet, P. Saint-Marc, and G. Medioni. B-snakes: Implementation and application to stereo. In *Proceedings of the DARPA Image Understanding Workshop, Pittsburgh, PA*, pages 720–726, Sept. 1990.
8. Michael E. Mortenson. *Geometric Modeling*. John Wiley and Sons, New York, 1985.
9. J. Park, D. Metaxas, and L. Axel. Volumetric deformable models with parameter functions: A new approach to the 3d motion analysis of the LV from MRI-SPAMM. In *International Conference on Computer Vision*, pages 700–705, 1995.
10. P. Radeva, A. Amini, and J. Huang. Deformable B-Solids and implicit snakes for 3D localization and tracking of SPAMM MRI data. *Computer Vision and Image Understanding*, 66(2):163–178, May 1997.
11. A. Young, D. Kraitchman, L. Dougherty, and L. Axel. Tracking and finite element analysis of stripe deformation in magnetic resonance tagging. *IEEE Transactions on Medical Imaging*, 14(3):413–421, September 1995.
12. E. Zerhouni, D. Parish, W. Rogers, A. Yang, and E. Shapiro. Human heart: Tagging with MR imaging – a method for noninvasive assessment of myocardial motion. *Radiology*, 169:59–63, 1988.